Rapidly Tunable Dual-Comb RF Photonic Filter for Ultrabroadband RF Spread Spectrum Applications

Hyoung-Jun Kim, Daniel E. Leaird, and Andrew M. Weiner

***Abstract*— We demonstrate a rapidly frequency-tunable radio frequency (RF) filter using microwave photonics technology for ultrawideband RF spread spectrum applications. A pair of electro-optic frequency combs is arranged as a dispersive tapped delay line in a differential detection configuration to implement a programmable finite impulse response RF filter. Our photonic scheme enables both fast frequency tuning on the order of tens of nanoseconds and wide tuning range (>7.5 GHz) with minimal variation of RF gain and passband shape. The low control voltage (ca. 1 V) and the linear relationship between control voltage and passband frequency facilitate agile frequency tuning for processing of signals with time-varying frequency content, while differential detection increases the photocurrent by a factor of two and suppresses common mode intensity noise. We exploit the rapid tunability of the implemented filter to demonstrate dynamic tracking of frequency-hopped and chirped RF signals. An experiment that performs dynamic filtering of an input chirp signal (3.92-GHz center frequency, up-chirped by >2 GHz within 100 ns) obscured by strong broadband noise achieves ∼11-dB signal-to-noise ratio (SNR) improvement. The SNR obtained is in addition to that available from standard matched filtering or pulse compression processing, suggesting strong potential for enhanced resistance against broadband noise jamming.**

***Index Terms*— Finite impulse response filters, frequency hopping, jamming, microwave photonic filter, microwave photonics, noise reduction, optical combs, programmable filters, spread spectrum, tunable filter.**

I. Introduction

FOR many decades, wireless technology has been significantly developed for a variety of wireless applications such as communications, sensing, imaging, and ranging. In addition, increasing radio frequency (RF) bandwidth is required for providing high speed and enhanced quality of wireless services. As wireless technology becomes more mature, the applications that utilize this technology in government, industry, and the military are requiring increasingly larger frequency resources for supporting broadband wireless services. However, the RF spectrum is crowded and frequently electromagnetic interference can be a significant problem, especially in unlicensed frequency bands. Also, jamming noise can be intentionally used to attack or interrupt electronic systems. In such harsh wireless environments, RF spread spectrum technology has been used for secure and reliable wireless communications because the signal-to-noise ratio (SNR) can be increased by a processing gain that is achievable using various frequency modulation and phase coding techniques [1]. For example, the IEEE 802.15 Task Group 4a selected chirp spread spectrum technology for wireless communication at the 2.4 GHz unlicensed band where interference is more severe [2]. In addition, frequency agility provides strong resistance to interference and jamming in wireless systems such as a cognitive radio and frequency-hopping spread spectrum [3], [4]. These systems can tune an operating RF frequency and thus can avoid jamming and interference.

For frequency-agile RF systems, a frequency-tunable RF filter is one of the key RF components and has been extensively developed by means of electronics and photonics technologies. In electronics, various tuning elements such as yttrium iron garnet (YIG) resonators, RF microelectromechanical systems (MEMS), and semiconductor varactor diodes have been used to design continuously tunable RF filters [5]–[13]. So far, the YIG filter has been widely and practically used because it has wideband tuning range capability and good selectivity [5]. However, it has a slow tuning speed on the order of milliseconds. The RF MEMS filter has high linearity and wide tuning range [6]–[11]. However, the tuning speed is slower than 1 μs [6]. The semiconductor varactor diode has a fast fundamental tuning speed in the order of nanoseconds [7], [12], [13]. However, the actual tuning speed of the varactor-based RF filter is limited by the time constant of the bias network. In [13], for example, the measured tuning speed in the RF filter was 120–720 ns for a 40-MHz frequency shift at a center frequency of 2.85 GHz. Because of the narrow capacitance range of varactor diodes, the filter tuning range was limited to <1 GHz. Furthermore, these filters require very high control voltage to adjust and actuate the varactor capacitance and MEMS diaphragm, respectively. The control voltage ranges are 0–30 V for varactor diodes and 0–120 V for MEMS [11], [12]. The tuning speed of the schemes is also limited by the bandwidth of a source or an amplifier requiring for generation of a high voltage control. In addition, the high control voltage change causes the nonlinear tuning relationship between the filter frequency and control voltage [12], [14].

Numerous schemes using photonics technology have been proposed and extensively investigated because they can

Manuscript received October 13, 2015; revised December 21, 2015 and July 2, 2016; accepted July 6, 2016. Date of publication September 5, 2016; date of current version October 4, 2016. This work was supported in part by the Office of the Assistant Secretary of Defense for Research and Engineering under the National Security Science and Engineering Faculty Fellowship program through Grant N00244-09-1-0068 from the Naval Postgraduate School and in part by the Basic Science Research Program through the National Research Foundation of Korea (NRF) funded by the Ministry of Education (NRF-2014R1A6A3A03059647). Any opinion, findings, and conclusions or recommendations expressed in this publication are those of the authors and do not necessarily reflect the views of the sponsors.

The authors are with the School of Electrical and Computer Engineering, Purdue University, West Lafayette, IN 47907-2035 USA (e-mail: sjun27@purdue.edu; leaird@purdue.edu; amw@purdue.edu).

Color versions of one or more of the figures in this paper are available online at http://ieeexplore.ieee.org.

Digital Object Identifier 10.1109/TMTT.2016.2599162

provide high flexibility over a large RF bandwidth. An earlier tapped delay line scheme based on a finite impulse response filter design utilized a single-wavelength laser and multiple delay lines [15]. In each of the delay lines that act as multiple filter taps, the filter taps for amplitude and phase can be controlled by the optical power and the length of the delay line, respectively. By setting the filter tap coefficient, this scheme has the potential to implement an arbitrary filter response over a large frequency range. However, it was difficult to control the filter tap coefficient and to scale the number of filter taps. Dispersive-tapped delay line schemes using multiwavelength sources and a single dispersive medium such as a dispersive fiber or chirped fiber Bragg grating have been proposed and demonstrated [16]–[21]. Among various multiwavelength sources, spectrally sliced noise sources and electro-optic (EO) frequency combs provide good scalability of the filter taps. The sliced noise source enables cost-effective filter implementation [19]–[21]. However, the incoherent property of the noise source limits filter RF performance. The EO comb source [22]–[29] provides one good choice for the dispersive-tapped delay line schemes [16] because it can provide many dozens of evenly spaced optical frequencies with gigahertz repetition rate, good spectral flatness, high coherence, and low noise. In conjunction with a programmable pulse shaper that enables precise control of the individual filter taps, programmable filters with arbitrary amplitude and phase responses can be realized [16], [30]–[32]. Although not adopted here, it is worth noting that through self-phase modulation-based spectral broadening of the EO comb in a highly nonlinear fiber, the number of optical comb lines and hence filter taps can be further increased, as in recent demonstrations of RF photonic phase filters with over 160 filter taps [30], [31].

In these schemes, frequency tuning has been achieved by means of a variable optical delay line or phase shaper within an interferometric configuration. Recently, Supradeepa *et al.* [33] introduced a dual-comb configuration to the dispersive-tapped delay line scheme, enabling fast filter frequency tuning in the order of tens of nanoseconds (<40 ns). However, because it was not optimized for RF performance, the RF insertion loss was high (e.g., ∼40 dB at 0.5-mA photocurrent). Furthermore, a periodic optical notch filter was implemented by a differential phase shift keying demodulator to eliminate a filter baseband response; during filter frequency tuning, it caused unwanted RF gain variations due to the periodic optical notch filter response.

In this paper, we demonstrate a rapidly frequency-tunable RF photonic filter using a dual-comb configuration for ultrawideband RF spread spectrum applications. Here, for the first time in this dual-comb scheme, we exploit differential detection, increasing RF gain by a factor of two and suppressing common mode intensity noise [20], [34], [35]. In addition, the optimization of the filter configuration using the dual-comb source provides much better RF gain; gain up to ∼1 dB is achieved, which is similar or slightly higher than that obtained with a single-comb source in [34] (e.g., RF gain ∼0 dB). Instead of the previous periodic optical notch filter, here we suppress the filter baseband response by setting the bias point of the Mach–Zehnder modulator (MZM) at minimum transmission. This eliminates any significant gain variation during tuning of the filter and also significantly reduces intensity noise [36], [37]. Unlike typical MEMS and varactor-based tunable filters, our scheme needs only a low control voltage (<2 V) and provides tuning that is substantially linear in the control voltage over a several gigahertz range.

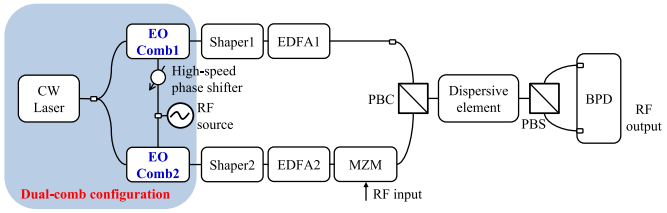

Fig. 1. Configuration of the RF photonic filter using dual-comb configuration and differential detection. PBC: polarization beam combiner and PBS: polarization beam splitter.

In this paper, for the first time, we begin to explore ultrabroadband RF spread spectrum applications of our rapidly tunable filter. We exploit the agility of the dual-comb filter to track frequency-swept or frequency-hopped RF signals over several gigahertz bandwidths on submicrosecond time scales. Proof-of-concept experiments using our agile dual-comb RF filter are successfully performed to track the instantaneous frequency of frequency-agile RF signals. Broadband noise that does not follow the frequency variation of the signal of interest is effectively suppressed because the instantaneous bandwidth of the tracking filter is narrower than the overall signal bandwidth. We perform a jamming experiment in which broadband noise is intentionally overlaid on a frequency-swept RF signal within a frequency range of 2.6-5.2 GHz; an SNR improvement of ∼11 dB is demonstrated through dynamic RF filtering. To the best of our knowledge, this is the first demonstration of submicrosecond dynamic RF filtering of frequency-swept RF signals for spread spectrum applications and systems.

The remainder of this paper is organized as follows. Section II describes our dual-comb RF photonic filter using a differential detection technique. In Section III, we present the concept of the dynamic RF filtering for ultrabroadband RF spread spectrum applications. The experiments and results are presented in Section IV. Section V describes practical considerations related to the dual-comb RF filtering scheme. Finally, we conclude this paper in Section VI.

II. Dual-Comb RF Photonic Filter

Figs. 1 and 2, respectively, show the configuration and a photo of the dual-comb RF photonic filter using differential detection. This filter configuration is based on our previous work on RF photonic filters reported in [33] and [34]. The novelty of our current implementation is that for the first time, we are able to simultaneously achieve attractive features shown separately in our previous filter designs, such as rapid frequency tuning in [33] and good RF metrics and frequency-independent RF gain in [34]. As shown in Fig. 1, we adopt the dual-comb configuration originally proposed in [33] for rapid frequency tuning. The dual-comb configuration enables high-speed optical delay control and thus results in rapid

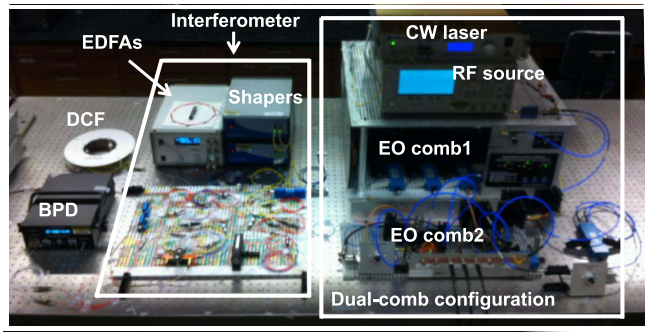

Fig. 2. Photograph of the RF photonic filter setup.

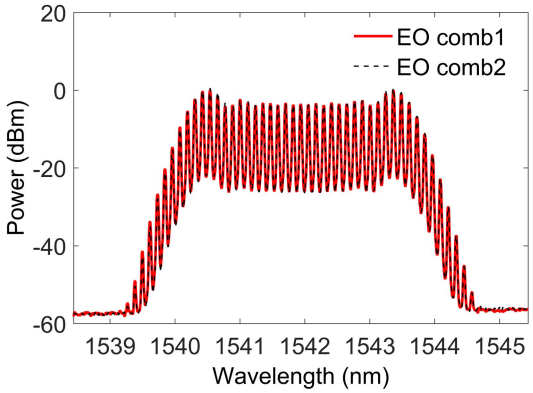

Fig. 3. Measured optical spectra at the outputs of the EO comb sources. The resolution of the optical spectrum analyzer is 0.05 nm.

filter frequency tuning on tens of nanosecond time scales. In addition, double-sideband modulation with suppressed carrier (DSB-SC) modulation and differential detection are used [34]. These techniques significantly suppress intensity noise, generating from the laser and optical amplifiers, and thus provide good RF metrics. In addition, the DSB-SC modulation solves large RF gain variations with respect to the filter center frequency, which was a problem of our previous comb-based filter designs with single-sideband modulation implemented by a single-sideband modulator and a periodic optical notch filter.

The dual-comb configuration consists of two EO frequency comb sources each having two phase modulators and one intensity modulator, additionally a high-speed and voltage-controlled RF phase shifter and an RF synthesizer [33]. A continuous-wave laser signal is split by an optical splitter and then directed to the two EO frequency comb sources. An RF tone is generated by an RF synthesizer, split by an RF power divider, and used to drive the two EO frequency comb sources. The high-speed voltage-controlled RF phase shifter connected to one of the RF power divider outputs is used at the RF input to one of the EO combs. Fig. 3 shows spectra of nearly identical optical frequency combs generated by the two EO comb sources. The RF phase shift in the RF phase shifter introduces an optical delay difference between the two optical frequency combs [33]. As a result, the tuning speed of our scheme depends on that of the RF phase shifter. The two frequency combs are identically shaped by the pulse shapers and amplified by the erbium-doped fiber amplifiers (EDFAs). The MZM biased at the minimum transmission is used in the lower arm, in which both the optical carriers and intensity noise coming from EDFA2 are suppressed. The delayed comb from the upper arm of the interferometer and the comb modulated by the RF signal of interest in the lower arm of the interferometer are controlled to have orthogonal polarizations and combined by a polarization beam combiner. The polarization-multiplexed signals are passed through a dispersive element and directed to a polarization beam splitter. The single dispersive element with polarization multiplexing is used to provide two nearly identical signal paths for differential detection [34]. Note that the principal axes of the polarization beam splitter following the dispersive element are aligned to have an angle of 45° to the polarization state of the signals coming from either the upper or lower arm of the interferometer. In this way the signal from the upper arm alone or from the lower arm alone is suppressed upon detection by the balanced photodetector (BPD), whereas the beat signal arising from the interference between the upper arm field and the lower arm field yields two complementary outputs that add upon differential detection.

The filter transfer function of this scheme can be expressed as [16], [34]

$$H(\omega_{\mathrm{RF}}) \propto \sum_{n}^{N} P_n \left[e^{j[n\Delta\omega(\psi_2\omega_{\mathrm{RF}} \pm \tau) \mp \varphi_n]} \right] \tag{1}$$

where P_n is the RF amplitude of the n^{th} tap, produced by beating the n^{th} optical carrier and n^{th} optical sideband; $\Delta\omega$ is the comb spacing (i.e., optical pulse repetition rate); ψ_2 is the coefficient for the second-order phase; τ is the delay difference between the two interferometer arms; and φ_n represents the phases applied to n^{th} optical comb line with the pulse shaper. Because the MZM generates optical double sidebands, there are two filter passband terms within one filter free spectral range (FSR $= 1/T$, where T is the filter differential tap delay), pointed out by the $\pm$ sign in (1) [34]. In (1), the first phase terms indicate that there are filter passbands due to the differential tap delay ($T = \psi_2\Delta\omega$), originating from the second-order dispersion of the dispersive element. Furthermore, the filter center frequency is tunable by varying the delay difference (τ). Due to the opposite sign, the two filter passbands are shifted in opposite directions. When the Nyquist zone (i.e., half of comb repetition rate) is wider than the filter FSR, the filter tuning range is limited by FSR/2 due to the optical double sidebands generated by the DSB-SC modulation. Using single sideband with suppressed carrier (SSB-SC) modulation that can be implemented by a dual-parallel MZM, the filter tuning range can be increased by a factor of two to the filter FSR.

As discussed before, the dual-comb filtering scheme adopts techniques to improve RF performance, such as DSB-SC modulation and differential photodetection, utilized in the single-comb filtering scheme [34]. However, due to the different comb configuration, the RF gain expression of the single-comb filtering scheme cannot be used in the dual-comb filtering scheme. Thus, we derive the RF gain of the dual-comb filtering

scheme through the same way presented in [34]. The peak RF gain in the filter passbands can be expressed as

$$G_{\mathrm{RF}} = \frac{P_{\mathrm{out}}}{P_{\mathrm{in}}} = \left(\frac{R\kappa\pi\alpha_F\sqrt{P_2 P_1 \alpha_{S1}\alpha_{S2} g_{A1} g_{A2} \alpha_M}}{2V_\pi} \right)^2 \quad (2)$$

where P_1 and P_2 are the total optical powers at the outputs of the EO comb sources; α_{S1} and α_{S2} are the loss factors of the pulse shapers; g_{A1} and g_{A2} are the gain factors of the EDFAs; α_M and α_F are the loss factors of the MZM and dispersive element, respectively; κ is the responsivity of the BPD; R is the impedance; and V_π is the half-wave voltage of the MZM. Using the total output photocurrent (I_{DC}), we can rewrite the peak RF gain as

$$G_{\mathrm{RF}} = \frac{\eta}{4\varepsilon(1+\eta)^2}\left(\frac{\pi I_{DC} R}{V_\pi}\right)^2 \quad (3)$$

where η ($=P_2\alpha_{S2}g_{A2}\varepsilon\alpha_M / P_1\alpha_{S1}g_{A1}$) is the ratio of the optical power at the MZM output (the lower arm of Fig. 1) to the optical power at the EDFA1 output (upper arm). ε is the ratio of minimum to maximum transmission of the MZM, which corresponds to a typical MZM extinction ratio specification. In previous RF photonic filtering and link schemes, various techniques using low biasing [38], optical filtering [39], and asymmetric input split ratio of an interferometer [34] have been used. Because these techniques suppress the optical carrier, the optical carrier-induced intensity noise is reduced. As a result, the noise figure can be improved. In addition, at fixed photocurrent, these techniques can increase RF gain by reducing the optical carrier to sideband power ratio (assuming that fixed photocurrent can be maintained, the optimum ratio is $\eta = 1$). In our scheme, since the optical carrier and sideband paths of the interferometer are separated, we can independently control the power of the optical carriers and sidebands through the optical gain of the EDFA1 and EDFA2, respectively. Note that all RF powers at the output of the BPD are reduced by a factor of four since the BPD has an internal matching resistor for maximum power transfer to a matched load and improved bandwidth [40]. However, photodetectors without the internal matching resistor are used to produce more power in some applications. Thus, the RF gain expression without the effect of the internal matching resistor has been used in RF photonics [31], [34], [40], [41]. All the numbers shown in this paper for output photocurrent, RF gain, and noise PSD refer to the values before the internal matching resistor. In other words, to account for the internal matching resistor, 6 dB is added to the power measured at the BPD output.

III. Concept of Dynamic RF Filtering for Ultrabroadband RF Spread Spectrum Signals

We now describe the concept of dynamic RF filtering for ultrabroadband RF spread spectrum signals with instantaneous frequency content that changes dynamically with time. For example, a frequency-hopped RF signal, where the center frequency of a narrowband channel is rapidly switched, is one type of dynamic RF signal. A narrowband tunable RF filter is required to track and filter out the frequency-hopping signal. This is a well-known example of dynamic RF filtering.

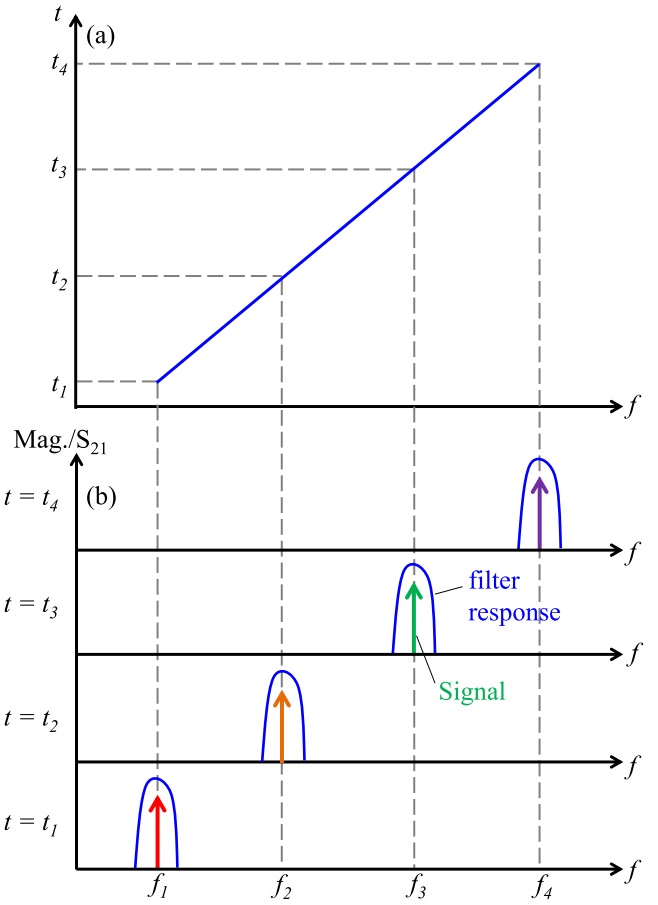

Fig. 4. Example of dynamic RF filtering for an up-chirp signal. (a) Signal chirp response. (b) Instantaneous signal spectra and filter responses at different times.

Here, we propose another novel example for dynamic RF filtering of a chirped spread spectrum signal; such chirped signals have been widely used in various RF spread spectrum applications [1]. As shown in Fig. 4(a), the instantaneous frequency of an up-chirp signal is increased from f_1 to f_4, as time increases from t_1 to t_4. Fig. 4(b) shows the instantaneous signal spectra and filter responses, showing the dynamic RF filtering process for the up-chirp signal. A narrowband tunable RF filter tracks and filters out the instantaneous signal frequency components. Unlike a conventional fixed wideband filtering approach, the dynamic RF filtering efficiently processes the up-chirp signal. In other words, it can suppress the noise or interference presented in a signal bandwidth. As a result, the SNR can be improved in harsh wireless environments where noise or interference is severe. A similar concept to dynamic RF filtering was proposed to filter out optical chirp pulses and to suppress amplified spontaneous noise through tunable optical filtering in chirped pulse amplification optical systems [42]. However, this concept was not presented for RF applications. To the best of our knowledge, here we physically implement and demonstrate submicrosecond dynamic RF filtering of multigigahertz RF chirp signals for the first time.

There are several considerations of tunable RF filters for dynamic RF filtering. First, the tunable RF filters should be faster than the signal frequency change. Second, constant filter characteristics over a large frequency tuning range are

TABLE I
FILTER CHARACTERISTICS FOR DIFFERENT FILTER PASSBANDS

Passband shapes	RF gain (dB)	Output noise (dBm/Hz)	NF (dB)	BW (GHz)	Sidelobe suppression (dB)
Sinc	0.8	-149.4	23.8	0.7	>12
Gaussian	1	-148	25	1.3	>30
Flat-top	0	-147.4	26.6	2.8	>24

NF: noise figure, BW: bandwidth

desirable during filter frequency tuning. Third, a low control voltage and linear relationship between the control voltage and filter frequency are also preferred for simple and high-speed frequency tuning control. Finally, in the presence of ultrabroadband jamming noise, the maximum achievable SNR improvement factor is approximately the ratio of the filter tuning range to filter bandwidth when the filter tuning range and noise bandwidth are the same. For high SNR improvement, narrow passband and wide tuning range are desirable.

IV. EXPERIMENT AND RESULTS

In this section, we first specify further details on the filter construction and then report the experimental results on the filter under static and dynamic operating conditions. Our implementation of the filter configuration of Fig. 1 starts with a continuous-wave laser with ∼2-W power that is split to feed two EO comb generators, each comprising two phase modulators and one intensity modulator driven by a constant 15-GHz RF tone. Each EO comb provides an output power of approximately 16 dBm. The half-wave voltage and extinction ratio of the MZM (EOSPACE AZ-1x2-8K8-20) in the lower arm of the interferometer are 3 V at 1 GHz and 20 dB, respectively. In this experiment, the optical carrier to sideband power ratio η is approximately 0.08. The dispersive element is a length of dispersion compensating fiber (DCF) with −400 ps/nm dispersion, which results in a filter FSR of 21.2 GHz. (For the jamming experiment, the DCF dispersion is changed to −1654 ps/nm, which results in a filter FSR of 5.23 GHz.) The EDFAs in the upper and lower interferometer arms compensate for the losses of optical components subsequent to the EO comb generators. In conjunction with the relatively high power provided at the output of the comb generators, this yields a photocurrent of ∼17 mA at the BPD (Discovery Semiconductors DSC720-HLPD), sufficient to obtain an RF gain near unity. The common mode rejection ratio at the output of the BPD is >30 dB after matching the optical powers and the lengths of the fiber leads connecting to the two inputs of the BPD. This provides sufficient suppression of the noise introduced in the EDFAs to achieve noise figures on the order of 25 dB, similar to what we reported in our previous work using a single input comb with balanced detection [34] and much better than what is often achieved with RF photonic filters. Examples of RF metrics are given in Table I.

A. Filter Characteristics

Compared with other schemes such as electronic filters and photonics-based schemes using high-Q optical resonators,

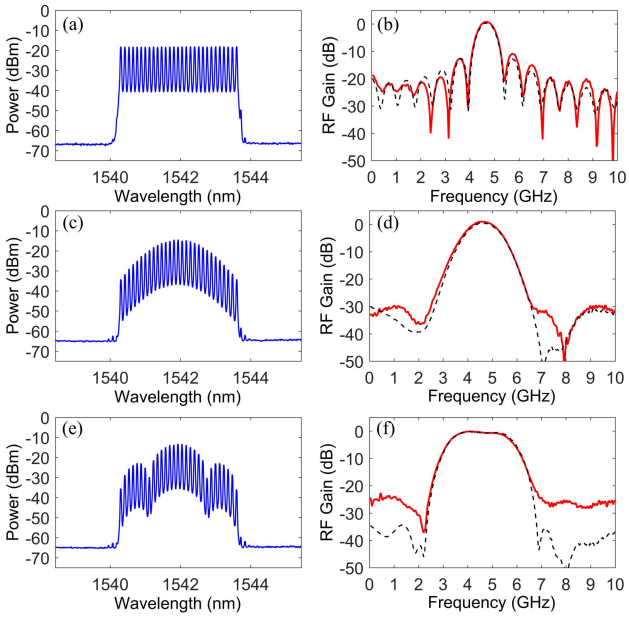

Fig. 5. Programmability of filter passband shapes. Measured optical spectra of combs with (a) flat-top, (c) Gaussian, and (e) Sinc (apodized by Kaiser window) envelopes, corresponding to the filter amplitude responses with (b) Sinc, (d) Gaussian, and (f) flat-top passbands, respectively. The resolution of the optical spectrum analyzer is 0.05 nm. In (b), (d), and (f), black dashed and red solid lines show simulation and measurement, respectively.

filter passband programmability is a unique advantage of comb-based RF photonic filters. This advantage is achieved because of the finite impulse response filter design, with filter coefficients easily controlled by the programmable pulse shaper. We have experimentally demonstrated the programmability of the filter passband in the single-comb filtering scheme using a single photodetector [16], [32]. However, RF performance metrics, e.g., RF gain, were not investigated in these studies. Here, we evaluate and compare RF metrics for different passband shapes in the dual-comb filtering scheme using differential detection. To show filter passband programmability, programmable pulse shapers (Finisar WaveShaper 1000S) are used to make different comb shapes with 29 comb lines. Fig. 5(a), (c), and (e) shows optical spectra at the output of pulse shaper1 for flat-top, Gaussian, and Sinc (with Kaiser window [32], [43]) shapes, respectively. The output comb shapes of both pulse shapers are close to identical. For the Sinc comb shape case, optical phases are applied in pulse shaper 2 to have 180° difference between the mainlobe and sidelobes. Based on (1), there is a Fourier transform relationship between the comb shape and filter passband shape. As a result, as shown in Fig. 5, the combs with flat-top, Gaussian, and Sinc shapes result in filter passbands with Sinc, Gaussian, and flat-top shapes, respectively. The measurements for the filter transfer function and RF gain agree with simulation calculated by (1) and (3), except for stopband suppression in the flat-top filter passband case as shown in Fig. 5(f). The stopband attenuation level difference of 7.5–13 dB between simulation and measurement may be caused by imperfect amplitude and phase errors in the control of the taps [32]. For different filter passbands, the RF gain is >0 dB with 1-dB variation. There is no significant change

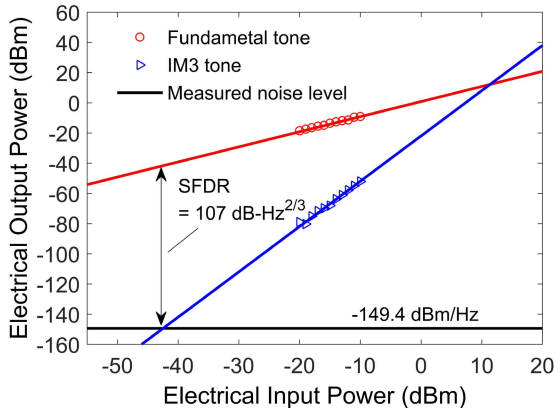

Fig. 6. Measured SFDR.

in the RF gain. It is because the saturated output powers of EDFA1 and EDFA2 produce the same photocurrent although shaping losses in the pulse shapers are slightly different for all filter passband cases. Note that the RF gain of the flat-top filter passband is ∼1 dB lower than that of other filter passbands due to the use of negative filter tap coefficients. The filter characteristics for the different filter passbands are summarized in Table I. The output noise variation for different filter passbands is 2 dB due to different apodization losses of the pulse shapers. As a result, noise figure variation among the different filter passbands is less than 3 dB. The 3-dB bandwidths, related to the comb shapes, are 0.7, 1.3, and 2.8 GHz for the Sinc, Gaussian, and flat-top passbands, respectively. Among the filter passbands, the Gaussian passband case has the largest sidelobe suppression (>30 dB).

Recently, Kim and Weiner [44] reported on intermodulation distortion characteristics of the filtering scheme using single-comb configuration and differential detection. A third-order spurious-free dynamic range (SFDR3) of 108.2 dB·Hz$^{2/3}$ at a filter center frequency of 4 GHz at an output photocurrent of ∼20 mA was achieved, with variation <1.2 dB for filter center frequencies from 2 to 7 GHz. Here we briefly report on the SFDR3 results of the dual-comb filtering scheme using differential detection. A two-tone test with the Sinc filter passband was performed to evaluate linearity of our scheme. Both the filter center frequency and two-tone center frequency were set to 4.7 GHz. The two-tone spacing was 10 MHz. The third-order intermodulation tones (IM3s) at 4.695 and 4.705 GHz were generated at the filter output. As shown in Fig. 6, the electrical output power of the fundamental tone and IM3 increased with slopes of 1 and 3, respectively, as the input electrical power of the two tones increased. The SFDR3 of the dual-comb filter scheme is 107 dB·Hz$^{2/3}$, which is similar to the value achieved with the single-comb filter scheme. The SFDR3 is limited by photodetector nonlinearity at a high photocurrent level [44].

Fig. 7(a) shows the relationship between the filter center frequency and the control voltage to the RF phase shifter. As the control voltage is increased, the filter frequency is linearly increased with a slope of ∼6.94 GHz/V. Compared with a linear fit (black solid line), the measured tuning relationship (open symbols) has a standard deviation of 45 MHz.

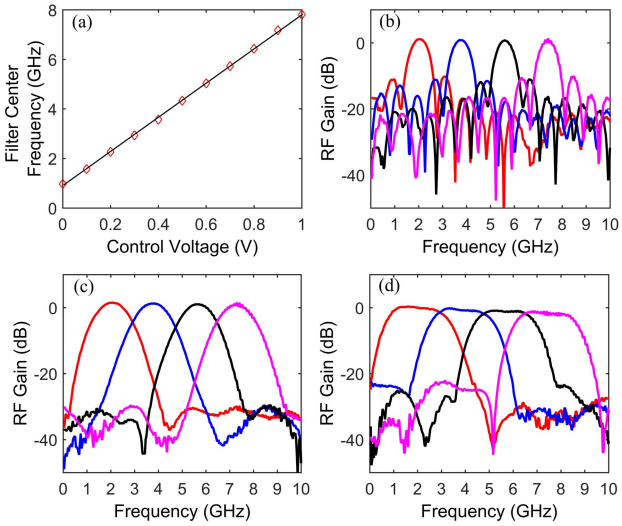

Fig. 7. Filter frequency tuning. (a) Filter center frequency as a function of a control voltage. Measured RF gain as a function of a frequency for (b) Sinc, (c) Gaussian, and (d) flat-top filter passband shapes.

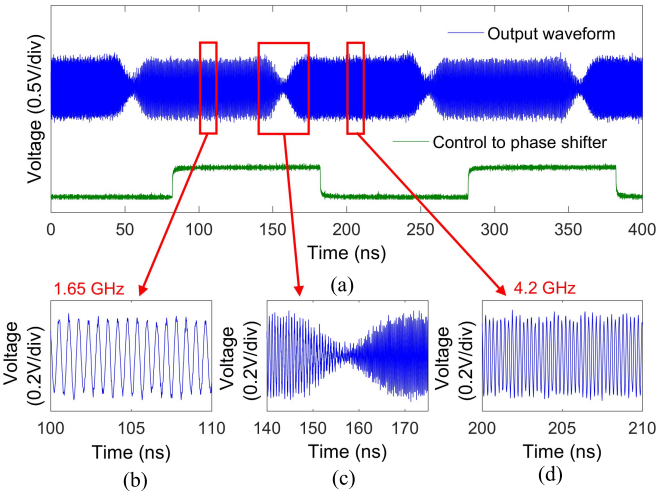

Fig. 8. Tuning speed of filter center frequency with dynamic tuning control. Input signal comprises superimposed 1.65-GHz and 4.2-GHz tones. (a) Waveforms of filter output (blue top curve) and control (green bottom curve) signals. (b) Zoom-in waveform with 1.65-GHz filter center frequency. (c) Zoom-in waveform when the filter center frequency is changed from 1.65 to 4.2 GHz. (d) Zoom-in waveform with 4.2-GHz filter center frequency.

Because the required voltage to tune the filter frequency from 1 to 8 GHz is ∼1 V, the full frequency tuning of filter FSR (21.2 GHz) requires <3 V. This indicates that the control voltage requirement of our scheme is much lower than those of varactor- and MEMS-based filters (<120 V) [11]. Due to the low control voltage and linear relationship between the control voltage and filter frequency, the filter frequency control is simplified. Fig. 7(b)–(d) shows the static filter frequency tuning for the different filter passbands with Sinc, Gaussian, and flat-top shapes, respectively. Tuning the filter center frequency from 2 to 7.4 GHz, the RF gain variations for the Sinc, Gaussian, and flat-top passband cases are <0.1, <0.5, and <1.3 dB, respectively. (Please note that although the filter frequency response is measured up to 10 GHz, the spurious-free frequency range comprising one Nyquist zone is only 0–7.5 GHz.) In addition to the filter characteristics with

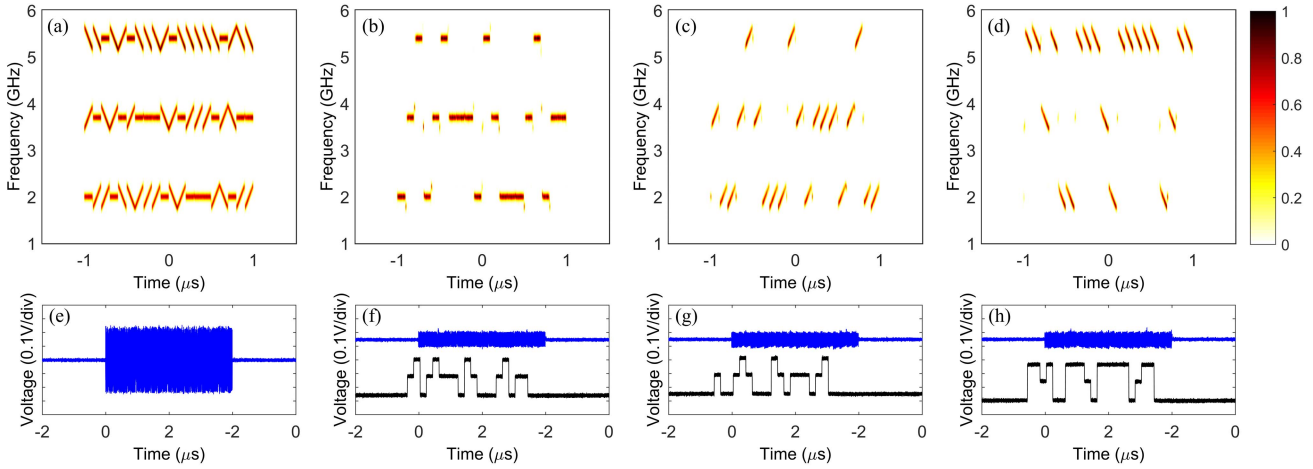

Fig. 9. Dynamic RF filtering for frequency-hopping spread spectrum signals. (a) and (e) Measured input waveform and normalized spectrogram. (b) and (f) Measured output waveform and normalized spectrogram for a single tone. (c) and (g) Measured output waveform and normalized spectrogram for an up-chirp. (d) and (h) Measured output waveform and normalized spectrogram for a down-chirp. In (f)–(h), top (blue) and bottom (black) curves show the output waveforms and control signals, respectively.

the static tuning, as shown in Fig. 8, we evaluate the tuning speed of our scheme with dynamic tuning control. Two RF tones at 1.65 and 4.2 GHz are generated and directed to the dual-comb RF photonic filter with the Gaussian filter passband. The control voltage to the RF phase shifter is a 5-MHz square wave that tunes the filter back and forth between the two input frequencies. When the filter frequency is switched from 1.65 to 4.2 GHz, the transition time is ∼20 ns.

B. Dynamic RF Filtering for RF Spread Spectrum Applications

Using our dual-comb RF photonic filter with the Gaussian filter shape, we first demonstrate processing of a frequency-hopped signal. Fig. 9 shows the input signal, output signals under different filter tunings, and corresponding normalized spectrograms. Spectrograms are an example of a joint time-frequency distribution, an analysis tool used to characterize signals for which the frequency content is varying in time [45]. In order to obtain the spectrogram plots of Fig. 9, we use a Gaussian gate function with 3-ns duration. An electronic RF arbitrary waveform generator provides a 2-μs duration input test signal, shown in Fig. 9(a) and (e), which overlays three distinct frequency-hopped waveforms. Within each 100-ns time interval, there are three distinct waveform types (one a single tone, one a 5-MHz/ns up-chirp, and one a −5 MHz/ns down-chirp) centered at three different RF frequencies (2, 4, and 6 GHz). The different waveforms types are chosen so that they can be easily distinguished in the spectrograms. Each waveform type may hop to a new center frequency at the start of each new 100-ns time interval, with the constraint that none of the waveforms are allowed to be at the same center frequency at the same time. Thus, the test signal may represent three different frequency-hopped communication channels sharing the same RF spectrum. The control voltages to the RF phase shifter, shown in Fig. 9(f)–(h), have three voltage levels corresponding to the three hop frequencies. As shown in Fig. 9(b)–(d), each waveform type is successfully tracked and selected using different control patterns. We see no evidence of hysteresis or memory effects in the filter tuning.

In another example, Fig. 10 shows the dynamic RF filtering of ultrawideband up-chirp and down-chirp signals. The filter shape is Gaussian. The Gaussian gate function of the spectrograms shown in Fig. 10 has 2-ns duration. The input signals shown in Fig. 10(a) and (c) have an RF bandwidth of 3.5 GHz and a chirp rate of ±1.75 GHz/μs for the up-chirp and down-chirp, respectively. As shown in Fig. 10(f) and (h), simple ramp control signals with positive and negative slopes are used to track and filter out the chirp signals, respectively. As a result, up-chirp and down-chirp signals are tracked and filtered using simple control waveforms with different slopes. This indicates that our scheme provides rapid reconfigurability by changing the control signal. Note that the peak amplitude of the output waveforms is reduced by a factor of two compared with the input waveforms due to the internal matching resistor loss (6 dB) of the BPD.

In addition, we perform an experiment in which dynamic RF filtering of an up-chirp signal provides an SNR improvement for resistance against broadband noise jamming. To maximize the SNR improvement, we change the DCF dispersion from −400 to −1654 ps/nm, which results in a filter with FSR and 3-dB bandwidth reduced to ∼5.23 GHz and ∼200 MHz, respectively. Fig. 11 shows the experimental configuration. Fig. 12(a) shows the measured spectrum of the Gaussian-shaped optical comb. Fig. 12(b) shows the filter amplitude response with the passband tuned to 4 GHz. In the experiment, the filter is tuned over one-half of the filter FSR, i.e., from approximately 2.6 to 5.23 GHz. Note that the RF gain is reduced to −7 dB due to the increased loss associated with the longer length of DCF. However, the RF gain reduction can be compensated by replacing the DCF with a low-loss highly dispersive fiber Bragg grating [46]. The input up-chirp signal generated from an RF arbitrary waveform generator has an RF bandwidth of 2.17 GHz at 3.92-GHz center frequency

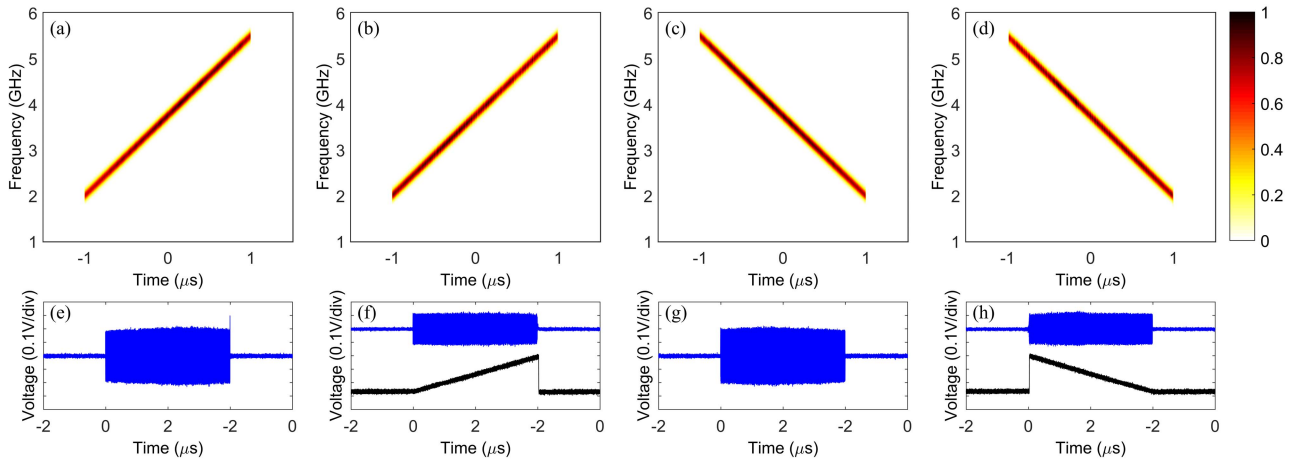

Fig. 10. Dynamic RF filtering for chirp spread spectrum signals with positive and negative chirp rates. (a) and (b) Normalized spectrograms of the measured input and output waveforms for the positive chirp rate, respectively. (c) and (d) Normalized spectrograms of the measured input and output waveforms for the negative chirp rate, respectively. (e) and (f) Measured input and output waveforms for the positive chirp rate, respectively. (g) and (h) Measured input and output waveforms for the negative chirp rate, respectively. In (f) and (h), top (blue) and bottom (black) curves show the output waveforms and control signals, respectively.

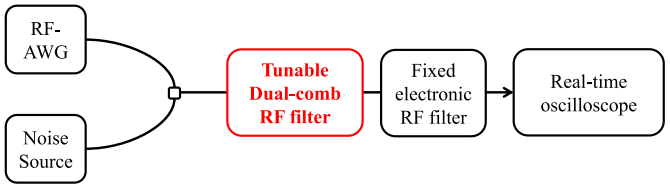

Fig. 11. Experimental setup for jamming noise suppression by dynamic RF filtering.

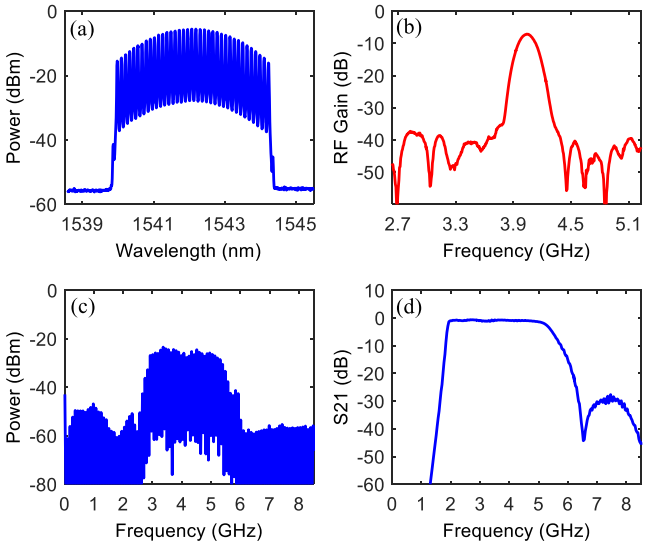

Fig. 12. (a) Measured spectrum of the shaped comb. (b) Measured amplitude response of the dual-comb RF filter. (c) Measured RF spectrum of the wideband noise. The resolution is 3 MHz. (d) Measured amplitude response of the fixed electronic RF filter.

and a time duration of 100 ns as shown in Fig. 13(a). Wideband noise is generated from cascaded RF amplifiers and filters with the input terminated in 50 Ω and combined with the up-chirp signal. Fig. 12(c) shows the RF spectrum of the wideband noise, where the 6-dB noise bandwidth is 2.38 GHz at a center frequency of 4.1 GHz. At the output of the dual-comb RF photonic filter, an additional fixed electronic RF filter shown in Fig. 12(d) is used to remove unwanted spurious signals outside of the filter tuning range. The 3-dB bandwidth of the fixed electronic filter is 3.4 GHz. A real-time oscilloscope is used to record the filtered signals for offline analysis.

Fig. 13 shows measured waveforms and their spectrograms at the input and output of the dual-comb RF filter. The Gaussian gate function used for the spectrograms shown in Fig. 13 has 4-ns duration. First, we evaluate the SNRs from the measured waveforms on a real-time oscilloscope. As shown in the inset of Fig. 13(a), without the noise, the input SNR is ∼22 dB. When the noise is added, the input signal is at most barely observable as shown in the inset of Fig. 13(b), where the input SNR is −1.1 dB. The signal can be discerned from the spectrogram plot of Fig. 13(b), but the strong noise background is equally apparent. The signal and noise are directed to the filter, and a triangular control waveform with 5-MHz period is applied to track the input up-chirp signal and filter out noise outside the instantaneous filter passband. In the spectrogram shown in Fig. 13(c), the filter tracking trace is clearly observed due to the corresponding time-dependent variation of the noise frequency transmitted. The shape is identical to and shares the same repetition rate as the control signal shown in the inset of Fig. 13(c). At the center of the spectrogram, the tracking path is exactly matched to the signal chirp. Thus, the dynamic RF filtering efficiently selects the signal component dynamically changing with time and suppresses the noise outside the instantaneous signal bandwidth. As a result, the output SNR is improved to approximately 9.86 dB, showing an SNR improvement of ∼11 dB.

Pulse compression of spread spectrum signals based on matched filtering has been widely used for RF applications in wireless communications and radar [1], [2], [4]. RF chirp signals, for example, are radiated from a transmitter and then compressed at a receiver via correlation processing. Compression may be performed using analog phase filters or

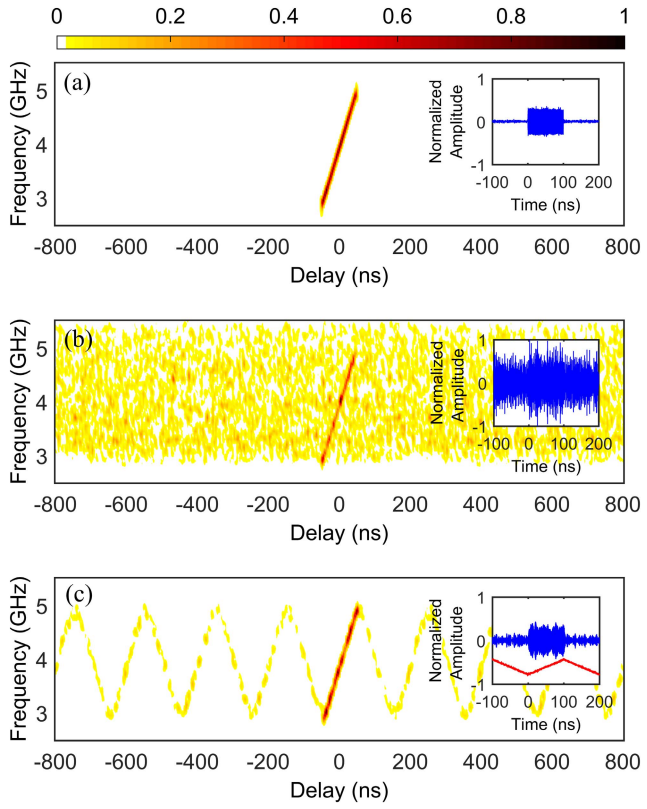

Fig. 13. Normalized spectrograms of (a) measured input waveform without the noise, (b) measured input waveform with the noise, and (c) measured output waveform with the noise. The insets of (a)–(c) show the corresponding normalized waveforms.

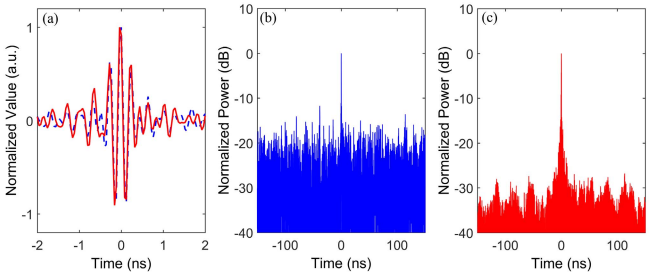

Fig. 14. Cross-correlations. Cross-correlation-1 is between the input waveform with noise and the reference waveform (the input chirp without added noise). Cross-correlation-2 is between the output of the dynamic filter when its input is the chirp waveform with additive noise and the same reference waveform (input chirp without noise). (a) Linear scales of cross-correlation-1 (blue dashed curve) and cross-correlation-2 (red curve). (b) Log scale of cross-correlation-1. (c) Log scale of cross-correlation-2.

via cross-correlation with a stored reference waveform using a digital signal processor. Here we examine compression of the chirp signal considered in the experiments of Figs. 11–13, with and without dual-comb RF photonic filtering. Compression is performed offline using the time-domain data from Fig. 13. Our results are shown in Fig. 14. The blue dashed lines indicate cross-correlation-1 between the input waveform with noise and the reference–the input waveform without noise. The red lines indicate cross-correlation-2 between the output of the dynamic filter when its input is the waveform with noise and the reference waveform (again the input chirp signal without added noise). As shown in Fig. 14(a), both cross-correlation traces shown on a linear scale appear to be symmetric and closely match. Thus, the compressibility of the chirp signal is not degraded by the dual-comb RF filter; no significant signal distortion is introduced during the dynamic RF filtering process. Fig. 14(b) and (c) shows the square of the computed cross-correlation traces on a logarithmic scale. Here we clearly observe that the compression result for the dynamically filtered chirp has much lower noise background than is observed for the unfiltered chirp plus noise. The difference in the background noise power level in time in Fig. 14(b) and (c) is close to the value of the SNR improvement reported above. Thus, the dynamic RF filtering technique as described here may be viewed as complementary to pulse compression, in that the SNR enhancements available individually from dynamic filtering or pulse compression when either is used alone appear to add when both techniques are used together.

Further enhancements should be possible if filtering is performed using combs with larger optical bandwidth. In the present experiments, the bandwidth of the EO comb is approximately 0.44 THz. However, similar combs with approximately five times larger optical bandwidth have been recently reported [29], [47]. Adopting such a wideband EO comb for our RF photonic filter with the parameters of the jamming experiment, the filter bandwidth should be reduced by a factor of five to about to 40 MHz. In this case, the quality factor of the filter would be approximately 200. The use of SSB-SC modulation in our filtering scheme should increase the filter tuning range by a factor of two. The combination of these two techniques should enable another 10-dB improvement in noise suppression compared with the results reported above.

V. Discussion

Here we briefly discuss several considerations relevant to practical applications. First, the bias point of the MZM may drift or be shifted by environmental changes, e.g., temperature. In our experiments, the effect of the bias drift was small for short-term measurements (10 min) [48]. However, over long time periods, the MZM bias point may deviate significantly from minimum transmission, increasing the filter baseband response and the intensity noise. Thus, for long-term operation, a bias controller is recommended to prevent MZM bias drift [48].

Second, micrometer scale length variations in our fiber-based interferometer lead to variations of the relative optical phase of the two interferometer arms. Such variations are converted into variations of the RF phase upon photodetection (without, however, significantly changing the RF filter response). If low-frequency RF phase fluctuations are not acceptable, then the interferometer needs stabilization. This can be achieved using a piezo controller inside the interferometer, similar to the stabilization of the fiber-based interferometer used for RF arbitrary waveform generation in [49], or through integration.

Finally, translation of our scheme to integrated photonics would substantially benefit stability and would be highly desirable to reduce the physical footprint and cost. Indeed, photonic integration has assumed a prominent role in microwave

photonics research within the last few years [50], [51]. Integration of a structure as complex as that shown in Fig. 1 is challenging and will not happen immediately. However, progress in the field of integrated photonics is rapid [52], [53]. Here we briefly mention progress in the integration of two of the more complex optical functionalities needed for our RF photonic filtering scheme, the comb generators and the pulse shapers. For the comb generation functionality, nonlinear wave mixing mediated by the optical Kerr effect within a high quality factor microresonator pumped by a single-frequency laser is promising [54]. Such Kerr combs have been demonstrated to provide dozens to hundreds of comb lines at repetition rates of tens to hundreds of gigahertz (high repetition frequency is an advantage for RF photonic filtering) with low noise and high optical coherence. RF photonic filter experiments using Kerr combs generated from optical microresonators fabricated on silicon photonic chips have been reported in [55] and [56]; wavelength-division multiplexed coherent optical communications experiments have also been reported using combs generated from such chip-scale microresonators [57]. Tuning schemes for such Kerr combs, which are relevant to achieving RF filter tuning in RF photonic filter implementations, are now beginning to be explored [58]. In addition, a number of papers discussing integrated pulse shapers have been reported [59]–[64], with material platforms including silica [59], silicon [60], and InP [61]–[64]. Pulse shapers fabricated in silica have been demonstrated with up to 64 channels with both amplitude and phase controlled thermo-optically, providing millisecond-scale reprogramming [62]. InP platforms offer the potential for much faster response as well as on-chip optical amplification. In one recent experiment, reconfiguration of a 32-channel amplitude pulse shaper was demonstrated with submicrosecond reprogramming time [64]. With such speeds available, reconfiguration of RF photonic filter responses will become possible via direct reprogramming of the pulse shaper itself (see [65] for a preliminary demonstration).

VI. Conclusion

We demonstrate a dual-comb RF photonic filter with differential detection for ultrabroadband RF spread spectrum applications. This scheme provides several advantages. First, the dual-comb configuration enables fast frequency tuning on the order of tens of nanoseconds. Second, the filter optimization with differential detection improves filter RF performance. Third, our scheme has a wide filter tuning range and constant filter characteristics. Finally, low control voltage requirement and linear relationship between the control voltage and filter frequency simplify filter frequency control. Using this scheme, we demonstrate submicrosecond dynamic RF filtering of frequency-swept or frequency-hopped signals. In the presence of ultrawideband jamming noise, the dynamic RF filtering with a chirp signal improves the SNR by $\sim$11 dB. These results show interesting potential for ultrabroadband frequency-agile RF applications.

Acknowledgment

The authors would like to thank Dr. J. D. McKinney and Dr. X. Xue for helpful technical discussions. Any opinion, findings, and conclusions or recommendations expressed in this publication are those of the authors and do not necessarily reflect the views of the sponsors.

References

[1] M. K. Simon, J. K. Omura, R. A. Scholtz, and B. K. Levitt, *Spread Spectrum Communications Handbook*. New York, NY, USA: McGraw-Hill, 1994.

[2] E. Karapistoli, F.-N. Pavlidou, I. Gragopoulos, and I. Tsetsinas, "An overview of the IEEE 802.15.4a standard," *IEEE Commun. Mag.*, vol. 48, no. 1, pp. 47–53, Jan. 2010.

[3] S. Haykin, "Cognitive radio: Brain-empowered wireless communications," *IEEE J. Sel. Areas Commun.*, vol. 23, no. 2, pp. 201–220, Feb. 2005.

[4] R. Pickholtz, D. Schilling, and L. Milstein, "Theory of spread-spectrum communications—A tutorial," *IEEE Trans. Commun.*, vol. COM-30, no. 5, pp. 855–884, May 1982.

[5] J. Uher and W. J. R. Hoefer, "Tunable microwave and millimeter-wave band-pass filters," *IEEE Trans. Microw. Theory Techn.*, vol. 39, no. 4, pp. 643–653, Apr. 1991.

[6] G. M. Rebeiz, *RF MEMS: Theory, Design, and Technology*. New York, NY, USA: Wiley, 2003.

[7] G. M. Rebeiz *et al.*, "Tuning in to RF MEMS," *IEEE Microw. Mag.*, vol. 10, no. 6, pp. 55–72, Oct. 2009.

[8] S.-J. Park, I. Reines, C. Patel, and G. M. Rebeiz, "High-Q RF-MEMS 4–6-GHz tunable evanescent-mode cavity filter," *IEEE Trans. Microw. Theory Techn.*, vol. 58, no. 2, pp. 381–389, Feb. 2010.

[9] J. Small, M. S. Arif, A. Fruehling, and D. Peroulis, "A tunable miniaturized RF MEMS resonator with simultaneous high Q (500–735) and fast response speed (< 10–60μs)," *J. Microelectromech. Syst.*, vol. 22, no. 2, pp. 395–405, Apr. 2013.

[10] K. Chen, X. Liu, A. Kovacs, W. J. Chappell, and D. Peroulis, "Antibiased electrostatic RF MEMS varactors and tunable filters," *IEEE Trans. Microw. Theory Techn.*, vol. 58, no. 12, pp. 3971–3981, Dec. 2010.

[11] X. Liu, L. P. B. Katehi, W. J. Chappell, and D. Peroulis, "High-Q tunable microwave cavity resonators and filters using SOI-based RF MEMS tuners," *J. Microelectromech. Syst.*, vol. 19, no. 4, pp. 774–784, Aug. 2010.

[12] A. R. Brown and G. M. Rebeiz, "A varactor-tuned RF filter," *IEEE Trans. Microw. Theory Techn.*, vol. 48, no. 7, pp. 1157–1160, Jul. 2000.

[13] S. Sirci, J. D. Martínez, M. Taroncher, and V. E. Boria, "Low loss tunable filters in substrate integrated waveguide," *Waves*, vol. 1, no. 4, pp. 69–78, 2012.

[14] X. Liu, L. P. B. Katehi, W. J. Chappell, and D. Peroulis, "A 3.4–6.2 GHz continuously tunable electrostatic MEMS resonator with quality factor of 460–530," in *IEEE MTT-S Int. Microw. Symp. Dig.*, Jun. 2009, pp. 1149–1152.

[15] J. Capmany and D. Novak, "Microwave photonics combines two worlds," *Nature Photon.*, vol. 1, no. 6, pp. 319–330, Apr. 2007.

[16] E. Hamidi, D. E. Leaird, and A. M. Weiner, "Tunable programmable microwave photonic filters based on an optical frequency comb," *IEEE Trans. Microw. Theory Techn.*, vol. 58, no. 11, pp. 3269–3278, Nov. 2010.

[17] A. Ortigosa-Blanch, J. Mora, J. Capmany, B. Ortega, and D. Pastor, "Tunable radio-frequency photonic filter based on an actively mode-locked fiber laser," *Opt. Lett.*, vol. 31, no. 6, pp. 709–711, Mar. 2006.

[18] Y. Dai and J. Yao, "Nonuniformly-spaced photonic microwave delay-line filter," *Opt. Exp.*, vol. 16, no. 7, pp. 4713–4718, Mar. 2008.

[19] X. Xue, X. Zheng, H. Zhang, and B. Zhou, "Highly reconfigurable microwave photonic single-bandpass filter with complex continuous-time impulse responses," *Opt. Exp.*, vol. 20, no. 24, pp. 26929–26934, 2012.

[20] X. Xue, X. Zheng, H. Zhang, and B. Zhou, "Spectrum-sliced microwave photonic filter with an improved dynamic range based on a $LiNbO_3$ phase modulator and balanced detection," *IEEE Photon. Technol. Lett.*, vol. 24, no. 9, pp. 775–777, May 1, 2012.

[21] J. Mora *et al.*, "Automatic tunable and reconfigurable fiber-optic microwave filters based on a broadband optical source sliced by uniform fiber Bragg gratings," *Opt. Exp.*, vol. 10, no. 22, pp. 1291–1298, Nov. 2002.

[22] A. J. Metcalf, V. Torres-Company, D. E. Leaird, and A. M. Weiner, "High-power broadly tunable electrooptic frequency comb generator," *IEEE J. Sel. Topics Quantum Electron.*, vol. 19, no. 6, Nov./Dec. 2013, Art. no. 3500306.

[23] R. Wu, V. R. Supradeepa, C. M. Long, D. E. Leaird, and A. M. Weiner, "Generation of very flat optical frequency combs from continuous-wave lasers using cascaded intensity and phase modulators driven by tailored radio frequency waveforms," *Opt. Lett.*, vol. 35, no. 19, pp. 3234–3236, Oct. 2010.

[24] R. Wu, C. M. Long, D. E. Leaird, and A. M. Weiner, "Directly generated Gaussian-shaped optical frequency comb for microwave photonic filtering and picosecond pulse generation," *IEEE Photon. Technol. Lett.*, vol. 24, no. 17, pp. 1484–1486, Sep. 1, 2012.

[25] T. Yamamoto, T. Komukai, K. Suzuki, and A. Takada, "Spectrally flattened phase-locked multi-carrier light generator with phase modulators and chirped fibre Bragg grating," *Electron. Lett.*, vol. 43, no. 19, pp. 1040–1042, Sep. 2007.

[26] T. Sakamoto, T. Kawanishi, and M. Izutsu, "Asymptotic formalism for ultraflat optical frequency comb generation using a Mach–Zehnder modulator," *Opt. Lett.*, vol. 32, no. 11, pp. 1515–1517, Jun. 2007.

[27] I. L. Gheorma and G. K. Gopalakrishnan, "Flat frequency comb generation with an integrated dual-parallel modulator," *IEEE Photon. Technol. Lett.*, vol. 19, no. 13, pp. 1011–1013, Jul. 1, 2007.

[28] A. K. Mishra *et al.*, "Flexible RF-based comb generator," *IEEE Photon. Technol. Lett.*, vol. 25, no. 7, pp. 701–704, Apr. 1, 2013.

[29] A. Ishizawa *et al.*, "Phase-noise characteristics of a 25-GHz-spaced optical frequency comb based on a phase- and intensity-modulated laser," *Opt. Exp.*, vol. 21, no. 24, pp. 29186–29194, 2013.

[30] M. Song, V. Torres-Company, R. Wu, A. J. Metcalf, and A. M. Weiner, "Compression of ultra-long microwave pulses using programmable microwave photonic phase filtering with > 100 complex-coefficient taps," *Opt. Exp.*, vol. 22, no. 6, pp. 6329–6338, 2014.

[31] H.-J. Kim, A. Rashidinejad, and A. M. Weiner, "Low-loss ultrawideband programmable RF photonic phase filter for spread spectrum pulse compression," *IEEE Trans. Microw. Theory Techn.*, vol. 62, no. 12, pp. 4178–4187, Dec. 2015.

[32] M. Song, C. M. Long, R. Wu, D. Seo, D. E. Leaird, and A. M. Weiner, "Reconfigurable and tunable flat-top microwave photonic filters utilizing optical frequency combs," *IEEE Photon. Technol. Lett.*, vol. 23, no. 21, pp. 1618–1620, Nov. 1, 2011.

[33] V. R. Supradeepa *et al.*, "Comb-based radiofrequency photonic filters with rapid tunability and high selectivity," *Nature Photon.*, vol. 6, pp. 186–194, Feb. 2012.

[34] H.-J. Kim, D. E. Leaird, A. J. Metcalf, and A. M. Weiner, "Comb-based RF photonic filters based on interferometric configuration and balanced detection," *J. Lightw. Technol.*, vol. 32, no. 20, pp. 3478–3488, Oct. 15, 2014.

[35] X. Xue, X. Zheng, H. Zhang, and B. Zhou, "Noise reduction by balanced detection in microwave photonic filters based on optical broadband sources," in *Proc. Conf. Lasers Electro-Opt. (CLEO)*, 2011, p. CThY3.

[36] C. Middleton and R. Desalvo, "High performance microwave photonic links using double sideband suppressed carrier modulation and balanced coherent heterodyne detection," in *Proc. IEEE Military Commun. Conf.*, Oct. 2009, pp. 1–6.

[37] E. Hamid, R. Wu, V. R. Supradeepa, C. M. Long, D. E. Leaird, and A. M. Weiner, "Tunable radio frequency photonic filter based on intensity modulation of optical combs," in *Proc. IEEE Topical Meeting Microw. Photon. (MWP)*, Oct. 2010, pp. 393–396.

[38] E. I. Ackerman *et al.*, "Signal-to-noise performance of two analog photonic links using different noise reduction techniques," in *IEEE MTT-S Int. Microw. Symp. Dig.*, Jun. 2007, pp. 51–54.

[39] A. Perentos *et al.*, "Variable carrier reduction in radio-over-fiber systems for increased modulation efficiency using a Si_3N_4 tunable extinction ratio ring resonator," *Opt. Exp.*, vol. 20, no. 23, pp. 25478–25488, 2012.

[40] S. Iezekiel, *Microwave Photonics: Devices and Applications*. New York, NY, USA: Wiley, 2009, pp. 150–152.

[41] C. H. Cox, *Analog Optical Links*. Cambridge, U.K.: Cambridge Univ. Press, 2004.

[42] Z. Ma and S. Li, "Theoretical analysis of ASE contrast improvement with a rapid scanning F-P interferometer in a CPA system," *J. Opt.*, vol. 14, no. 7, 2012, Art. no. 075202.

[43] F. J. Harris, "On the use of windows for harmonic analysis with the discrete Fourier transform," *Proc. IEEE*, vol. 66, no. 1, pp. 51–83, Jan. 1978.

[44] H.-J. Kim and A. M. Weiner, "Intermodulation distortion of a comb-based RF photonic filter using balanced detection," *IEEE Photon. Technol. Lett.*, vol. 27, no. 23, pp. 2477–2480, Dec. 1, 2015.

[45] A. M. Weiner, *Ultrafast Optics*. New York, NY, USA: Wiley, 2009.

[46] C. Wang and J. Yao, "Fiber Bragg gratings for microwave photonics subsystems," *Opt. Exp.*, vol. 21, no. 19, pp. 22868–22884, Sep. 2013.

[47] T. Nishikawa, A. Ishizawa, M. Yan, H. Gotoh, T. W. Hänsch, and N. Picqué, "Broadband dual-comb spectroscopy with cascaded-electro-optic-modulator-based frequency combs," in *Proc. Conf. Lasers Electro-Opt. (CLEO)*, May 2015, pp. 1–2.

[48] J. Švarný, "Analysis of quadrature bias-point drift of Mach–Zehnder electro-optic modulator," in *Proc. Biennial Baltic Electron. Conf.*, Oct. 2010, pp. 231–234.

[49] A. Rashidinejad and A. M. Weiner, "Photonic radio-frequency arbitrary waveform generation with maximal time-bandwidth product capability," *J. Lightw. Technol.*, vol. 32, no. 20, pp. 3383–3393, Oct. 15, 2014.

[50] D. Marpaung, C. Roeloffzen, R. Heideman, A. Leinse, S. Sales, and J. Capmany, "Integrated microwave photonics," *Lasers Photon. Rev.*, vol. 7, no. 4, pp. 506–538, Jul. 2013.

[51] S. Iezekiel, M. Burla, J. Klamkin, D. Marpaung, and J. Capmany, "RF engineering meets optoelectronics: Progress in integrated microwave photonics," *IEEE Microw. Mag.*, vol. 16, no. 8, pp. 28–45, Sep. 2015.

[52] F. A. Kish *et al.*, "Current status of large-scale InP photonic integrated circuits," *IEEE J. Sel. Topics Quantum Electron.*, vol. 17, no. 6, pp. 1470–1489, Nov./Dec. 2011.

[53] M. J. R. Heck *et al.*, "Hybrid silicon photonic integrated circuit technology," *IEEE J. Sel. Topics Quantum Electron.*, vol. 19, no. 4, Jul./Aug. 2013, Art. no. 6100117.

[54] T. J. Kippenberg, R. Holzwarth, and S. A. Diddams, "Microresonator-based optical frequency combs," *Science*, vol. 332, no. 6029, pp. 555–559, Apr. 2011.

[55] X. Xue *et al.*, "Programmable single-bandpass photonic RF filter based on Kerr comb from a microring," *J. Lightw. Technol.*, vol. 32, no. 20, pp. 3557–3565, Oct. 15, 2014.

[56] T. G. Nguyen *et al.*, "Integrated frequency comb source based Hilbert transformer for wideband microwave photonic phase analysis," *Opt. Exp.*, vol. 23, no. 17, pp. 22087–22097, 2015.

[57] J. Pfeifle *et al.*, "Coherent terabit communications with microresonator Kerr frequency combs," *Nature Photon.*, vol. 8, pp. 375–380, Apr. 2014.

[58] X. Xue *et al.*, "Mode-locked dark pulse Kerr combs in normal-dispersion microresonators," *Nature Photon.*, vol. 9, pp. 594–600, Aug. 2015.

[59] D. J. Geisler *et al.*, "Modulation-format agile, reconfigurable Tb/s transmitter based on optical arbitrary waveform generation," *Opt. Exp.*, vol. 17, no. 18, pp. 15911–15925, 2009.

[60] M. H. Khan *et al.*, "Ultrabroad-bandwidth arbitrary radiofrequency waveform generation with a silicon photonic chip-based spectral shaper," *Nature Photon.*, vol. 4, no. 2, pp. 117–122, Feb. 2010.

[61] M. J. R. Heck *et al.*, "Design, fabrication and characterization of an InP-based tunable integrated optical pulse shaper," *IEEE J. Quantum Electron.*, vol. 44, no. 4, pp. 370–377, Apr. 2008.

[62] F. M. Soares *et al.*, "Monolithic InP 100-channel × 10-GHz device for optical arbitrary waveform generation," *IEEE Photon. J.*, vol. 3, no. 6, pp. 975–985, Dec. 2011.

[63] S. Tahvili *et al.*, "InP-based integrated optical pulse shaper: Demonstration of chirp compensation," *IEEE Photon. Technol. Lett.*, vol. 25, no. 5, pp. 450–453, Mar. 1, 2013.

[64] A. J. Metcalf *et al.*, "32 channel, 25 GHz InP integrated pulse shaper with SOA amplitude control," in *Proc. IEEE Photon. Soc. (IPC)*, Oct. 2015, pp. 500–501.

[65] H.-J. Kim *et al.*, "Comb-based programmable RF photonic filter with an InP arrayed waveguide grating pulse shaper," in *Proc. Conf. Lasers Electro-Opt. (CLEO)*, 2016, p. SF1G.2.

Hyoung-Jun Kim received the B.S. degree in electrical engineering from Kwangwoon University, Seoul, South Korea, in 2005. He received the M.S. and Ph.D. degrees in electrical engineering from the Gwangju Institute of Science and Technology, Gwangju, South Korea, in 2007 and 2011, respectively.

He has been a Post-Doctoral Researcher with the Ultrafast Optics and Optical Fiber Communications Laboratory, Purdue University, West Lafayette, IN, USA, since 2012. His current research interests include microwave photonics, photonic signal processing, microwave and photonic integrated circuits, millimeter-wave radio access networks using radio-over-fiber, and optical frequency comb generation.

Dr. Kim was the recipient of the Best Student Paper Award of the Global Symposium on Millimeter Waves in 2008, the Excellent Research Award in 2011 for his Ph.D. dissertation, and the Korean Government fellowships for National Research Graduate in 2009 and the Post-Doctoral Fellow in 2014. He serves as a Reviewer for *Optics Express*, the IEEE PHOTONICS TECHNOLOGY LETTERS, and the IEEE PHOTONICS JOURNAL.

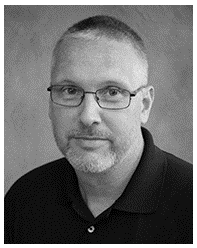

Daniel E. Leaird was born in Muncie, IN, USA, in 1964. He received the B.S. degree in physics from Ball State University, Muncie, in 1987, and the M.S. and Ph.D. degrees from the School of Electrical and Computer Engineering, Purdue University, West Lafayette, IN, USA, in 1996 and 2000, respectively.

He joined Bell Communications Research (Bellcore), Red Bank, NJ, USA, as a Senior Staff Technologist in 1987, and later advanced to a Member of Technical Staff. From 1987 to 1994, he was with the Ultrafast Optics and Optical Signal Processing Research Group, Purdue University, where he was a Key Team Member in Research Projects in Ultrafast Optics, such as shaping of short optical pulses using liquid crystal modulator arrays, investigation of dark soliton propagation in optical fibers, impulsive stimulated Raman scattering in molecular crystals, and all-optical switching. He has been a Senior Research Scientist and the Laboratory Manager of the Ultrafast Optics and Optical Fiber Communications Laboratory, School of Electrical and Computer Engineering, Purdue University, since 1994. He has co-authored nearly 120 journal articles and 160 conference proceedings. He holds three issued U.S. patents.

Dr. Leaird was the recipient of several awards for his work in the ultrafast optics field including a Purdue Professional Achievement Award, a Magoon Award for outstanding teaching, an Optical Society of America/New Focus Student Award, and a Bellcore "Award of Excellence." He is active in the optics community and professional organizations including the Optical Society of America and the IEEE Photonics Society, where he served as the Chair of the Ultrafast Optics Technical Committee from 2006 to 2009, and serves as a Consultant to venture capitalists by performing technical due diligence. He also serves as a Reviewer for *Optics Letters*, *Optics Express*, *Photonics Technology Letters*, *Applied Optics*, and the *Journal of the Optical Society of America B* in addition to serving on the National Science Foundation review panels in the SBIR program.

Andrew M. Weiner received the D.Sc. degree in electrical engineering from the Massachusetts Institute of Technology, Cambridge, MA, USA, in 1984.

He joined Purdue University, West Lafayette, IN, USA, as a Professor in 1992, and has since then graduated over 35 Ph.D. students. He joined Bell Communications Research (a premier telecommunications industry research organization), Red Bank, NJ, USA, initially as a Member of Technical Staff and later as the Manager of Ultrafast Optics and Optical Signal Processing Research. He is the Scifres Family Distinguished Professor of Electrical and Computer Engineering at Purdue University. In 2008 he was elected to membership in the National Academy of Engineering and in 2009 was named a Department of Defense National Security Science and Engineering Faculty Fellow. He has served a three-year term as the Chair of the National Academy's U.S. Frontiers of Engineering Meeting, and currently serves as the Editor-in-Chief of *Optics Express*, an all-electronic, open access journal publishing more than 3000 papers a year emphasizing innovations in all aspects of optics and photonics. He has also spent sabbaticals with the Max Born Institute for Nonlinear Optics and Ultrashort Pulse Spectroscopy, Berlin, Germany and with JILA, University of Colorado and National Institute of Standards and Technology, Boulder, CO, USA. He is especially well known for his pioneering work on programmable generation of arbitrary ultrashort pulse waveforms, which has found application both in fiber optic networks and in ultrafast optical science laboratories around the world. He authored the textbook *Ultrafast Optics*, 8 book chapters, over 300 journal articles, and over 500 conference papers. He holds 18 U.S. patents. His current research interests include ultrafast optics, with a focus on processing of extremely high-speed lightwave signals and ultrabroadband radio-frequency signals.

Prof. Weiner was the recipient of numerous awards, which include the Hertz Foundation Doctoral Thesis Prize in 1984, the Optical Society of America's Adolph Lomb Medal in 1990, the R. W. Wood Prize in 2008, the International Commission on Optics Prize in 1997, the IEEE Photonics Society's William Streifer Scientific Achievement Award in 1999, and the Quantum Electronics Prize in 2011. At Purdue University, he has been recognized with the inaugural Research Excellence Award from the School of Engineering in 2003, the Provost's Outstanding Graduate Student Mentor Award in 2008, the Herbert Newby McCoy Award for outstanding contributions to the natural sciences in 2013, and the College of Engineering Mentoring Award in 2014.